

Magnetic and Combined Field Integral Equations Based on the Quasi-Helmholtz Projectors

Adrien Merlini, *Student Member, IEEE*, Yves Beghein, Kristof Cools, Eric Michielssen, *Fellow, IEEE*, and Francesco P. Andriulli, *Senior Member, IEEE*

Abstract—Boundary integral equation methods for analyzing electromagnetic scattering phenomena typically suffer from several of the following problems: (i) ill-conditioning when the frequency is low; (ii) ill-conditioning when the discretization density is high; (iii) ill-conditioning when the structure contains global loops (which are computationally expensive to detect); (iv) incorrect solution at low frequencies due to current cancellations; (v) presence of spurious resonances. In this paper, quasi-Helmholtz projectors are leveraged to obtain a magnetic field integral equation (MFIE) formulation that is immune to drawbacks (i)–(iv). Moreover, when this new MFIE is combined with a regularized electric field integral equation (EFIE), a new quasi-Helmholtz projector combined field integral equation (CFIE) is obtained that also is immune to (v). Numerical results corroborate the theory and show the practical impact of the newly proposed formulations.

Index Terms—Electric, Magnetic, and Combined Field Integral Equations, Preconditioning, Calderon strategies.

I. INTRODUCTION

TIME-HARMONIC scattering by perfect electrically conducting (PEC) objects oftentimes is modeled using frequency-domain boundary integral equations. Among them, electric and magnetic field integral equations (EFIE and MFIE) [1] are the most popular.

Although the EFIE is easily discretized using Rao-Wilton-Glisson (RWG) basis functions [2], it suffers from ill-conditioning when the frequency is low and/or the discretization density is high. The MFIE, on the other hand, remains well-conditioned in both regimes, provided that a mixed discretization scheme is employed [3]. In practice, however, it is not feasible to obtain accurate results for the MFIE at extremely low frequencies without resorting to highly precise numerical quadrature methods. In addition to the above issues, both the EFIE and the MFIE suffer from current cancellations at low frequencies [4]–[6].

The EFIE's conditioning and current cancellation problems can be overcome by using loop-star or loop-tree decompositions [7]–[11]. For multiply connected geometries, this re-

quires the detection of global loops, which is computationally expensive [12]. These techniques also fail to address the dense discretization breakdown phenomena [13], [14] which causes the EFIE's condition number to grow quadratically with the mesh refinement parameter. Worse still, loop-star techniques for combatting the EFIE's low-frequency conditioning problems further degrade the equations dense discretization behavior [15].

Several formulations have been introduced to address these low-frequency issues without the computational burden of global loop detection [16], [17]. These solutions, however, do not address the dense discretization ill-conditioning of the EFIE. Both issues can be concurrently tackled by leveraging hierarchical quasi-Helmholtz decompositions [13], [18]–[20]. These decompositions also have been successfully coupled with other approaches such as Calderón preconditioning [14], [21]–[29] and Debye-inspired schemes [30]. The price to be paid for this dual stabilization is, once again, the need for global loop detection at very low frequencies. In addition, several of the aforementioned techniques fail to properly address low-frequency numerical cancellations occurring in the solution vector [4], [5], [31], [32]. Several of the above drawbacks have been successfully addressed by the promising scheme in [33]. Alternative remedies to current cancellations include perturbation methods [4], [31], [34] and Calderón regularization combined with loop star decompositions [25], [26]. Both families of solutions do, however, have shortcomings: the former is only applicable at low frequencies and exhibits the same spectral issues as the formulation it is applied to – high refinement breakdown for the EFIE or global loop detection for the MFIE and Calderón EFIE – while the latter also requires global loop detection and treatment of the high refinement instability of the loop-star decomposition. It should also be noted that some recent incarnations of augmented equations are immune to several of the above mentioned drawbacks, though they require the recovery of auxiliary quantities [35], [36].

Recently, an electric type equation based on quasi-Helmholtz projectors was proposed that is immune to all of the aforementioned issues [37]. A similar regularization has also been applied to the time domain electric field integral equation [38], [39] and both the time domain and the frequency domain PMCHWT equations [40], [41].

In this paper, quasi-Helmholtz projectors are used to obtain a new MFIE that no longer requires interaction integrals to be computed using extremely accurate quadrature rules. Additionally, the solenoidal and nonsolenoidal current com-

A. Merlini is with the Department of Electronics and Telecommunications of Politecnico di Torino, Turin, Italy (e-mail: adrien.merlini@polito.it).

Y. Beghein is with the Department of Information Technology (INTEC), Ghent University, 9502 Ghent, Belgium.

K. Cools is with the Department of Electrical Engineering, Delft University of Technology, Delft, Netherlands

E. Michielssen is with the Department of Electrical Engineering and Computer Science, University of Michigan, Ann Arbor, MI 48109, USA (e-mail: emichiel@umich.edu).

F. P. Andriulli is with the Department of Electronics and Telecommunications of Politecnico di Torino, Turin, Italy (e-mail: francesco.andriulli@polito.it).

ponents are scaled such that low frequency cancellations are avoided. As a result, the formulation remains accurate down to extremely low frequencies. Scattering problems involving PEC objects can also be solved using the combined field integral equation (CFIE), which is a linear combination of the EFIE and the MFIE. This equation has the added benefit that it does not support spurious resonances [42]. In this paper, the new regularization method for the MFIE is combined with that for the EFIE presented in [37]. The resulting CFIE is not only low-frequency stable but also immune to spurious resonances. Preliminary results of this research have previously been presented as conference contributions [43], [44].

This paper is organized as follows. To set notation, Section II defines the standard EFIE and MFIE as well as their discretizations and related quasi-Helmholtz current decompositions. In Section III, a quasi-Helmholtz decomposition is applied to a new symmetrized form of the MFIE. The resulting equation can be discretized accurately using standard numerical quadrature methods, and can be scaled in frequency such that no low frequency cancellations occur. In Section IV, this MFIE is combined with the regularized EFIE [37] to obtain an extremely low frequency stable CFIE. Section V discusses numerical results that corroborate the theory and conclusions are presented in Section VI.

II. BACKGROUND AND NOTATIONS

The EFIE and MFIE operators \mathcal{T}_k and \mathcal{K}_k are defined as

$$(\mathcal{T}_k \mathbf{j})(\mathbf{r}) = (\mathcal{T}_{s,k} \mathbf{j})(\mathbf{r}) + (\mathcal{T}_{h,k} \mathbf{j})(\mathbf{r}), \quad (1)$$

$$(\mathcal{T}_{s,k} \mathbf{j})(\mathbf{r}) = jk\eta \hat{\mathbf{n}} \times \int_{\Gamma} \frac{e^{-jkR}}{4\pi R} \mathbf{j}(\mathbf{r}') ds', \quad (2)$$

$$(\mathcal{T}_{h,k} \mathbf{j})(\mathbf{r}) = -\frac{\eta}{jk} \hat{\mathbf{n}} \times \nabla \int_{\Gamma} \frac{e^{-jkR}}{4\pi R} \nabla' \cdot \mathbf{j}(\mathbf{r}') ds', \quad (3)$$

$$(\mathcal{K}_k \mathbf{j})(\mathbf{r}) = -\hat{\mathbf{n}} \times p.v. \int_{\Gamma} \nabla \times \frac{e^{-jkR}}{4\pi R} \mathbf{j}(\mathbf{r}') ds', \quad (4)$$

where $R = \|\mathbf{r} - \mathbf{r}'\|$, Γ is the boundary of a closed domain $\Omega \subset \mathbb{R}^3$ and $\hat{\mathbf{n}}$ is its exterior normal vector. Furthermore, given the angular frequency ω , $k = \omega\sqrt{\mu\epsilon}$ and $\eta = \sqrt{\mu/\epsilon}$; here ϵ and μ the permittivity and permeability of vacuum, respectively. If Ω is perfectly conducting, it supports an electric current $\mathbf{j}(\mathbf{r})$ satisfying both the EFIE

$$(\mathcal{T}_k \mathbf{j})(\mathbf{r}) = \hat{\mathbf{n}} \times \mathbf{e}^i(\mathbf{r}) \quad (5)$$

and the MFIE

$$\left(\left(\frac{\mathcal{I}}{2} + \mathcal{K}_k \right) \mathbf{j} \right)(\mathbf{r}) = \hat{\mathbf{n}} \times \mathbf{h}^i(\mathbf{r}) \quad (6)$$

for all $\mathbf{r} \in \Gamma$; where \mathbf{e}^i and \mathbf{h}^i denote the impinging electric and magnetic fields, respectively. To numerically solve these equations via a Galerkin procedure, $\mathbf{j}(\mathbf{r})$ is expanded into RWG basis functions $\{\mathbf{f}_j(\mathbf{r})\}$ [2] as

$$\mathbf{j}(\mathbf{r}) \approx \sum_{j=1}^{N_e} [j]_j \mathbf{f}_j(\mathbf{r}), \quad (7)$$

where N_e is the number of edges of the mesh. Following [37], the RWG functions are normalized such that the integrated flux

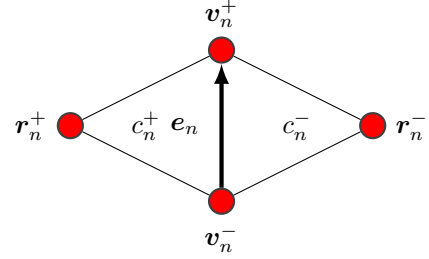


Figure 1. Notations used for the definition of an RWG basis function; \mathbf{e}_n denotes the defining inner edge that links vertices \mathbf{v}_n^+ and \mathbf{v}_n^- and \mathbf{c}_n^+ and \mathbf{c}_n^- the two triangles connected to this edge which are completed by the vertices \mathbf{r}_n^+ and \mathbf{r}_n^- , respectively.

through their defining edges equals one. Next, the EFIE (5) is tested with rotated RWG functions $\{\hat{\mathbf{n}} \times \mathbf{f}_i(\mathbf{r})\}$, while the MFIE (6) is tested with rotated Buffa-Christiansen (BC) functions [45] $\{\hat{\mathbf{n}} \times \mathbf{g}_i(\mathbf{r})\}$. The BC functions $\{\mathbf{g}_j\}$ are divergence-conforming functions defined on the barycentric refinement of the mesh. In addition, they are quasi curl-conforming in the sense that the mixed Gram matrix between curl-conforming rotated BC functions and RWG functions is well conditioned. For an explicit definition of these functions the reader is referred to [14], [45]. Overall, the testing procedure results in the following matrix equations:

$$\mathbf{T} \mathbf{j} = \mathbf{v}_e, \quad (8)$$

$$\left(\frac{\mathbf{G}^T}{2} + \mathbf{K}_k \right) \mathbf{j} = \mathbf{v}_h, \quad (9)$$

where

$$[\mathbf{T}]_{ij} = (\hat{\mathbf{n}} \times \mathbf{f}_i, \mathcal{T}_k \mathbf{f}_j), \quad (10)$$

$$[\mathbf{T}_s]_{ij} = (\hat{\mathbf{n}} \times \mathbf{f}_i, \mathcal{T}_{s,k} \mathbf{f}_j), \quad (11)$$

$$[\mathbf{T}_h]_{ij} = (\hat{\mathbf{n}} \times \mathbf{f}_i, \mathcal{T}_{h,k} \mathbf{f}_j), \quad (12)$$

$$[\mathbf{K}_k]_{ij} = (\hat{\mathbf{n}} \times \mathbf{g}_i, \mathcal{K}_k \mathbf{f}_j), \quad (13)$$

$$[\mathbf{G}]_{ij} = (\mathbf{f}_i, \hat{\mathbf{n}} \times \mathbf{g}_j), \quad (14)$$

$$[\mathbf{v}_e]_i = (\hat{\mathbf{n}} \times \mathbf{f}_i, \hat{\mathbf{n}} \times \mathbf{e}^i), \quad (15)$$

$$[\mathbf{v}_h]_i = (\hat{\mathbf{n}} \times \mathbf{g}_i, \hat{\mathbf{n}} \times \mathbf{h}^i), \quad (16)$$

with $(\mathbf{a}, \mathbf{b}) = \int_{\Gamma} \mathbf{a}(\mathbf{r}) \cdot \mathbf{b}(\mathbf{r}) ds$. In addition we denote by \mathbb{T} , \mathbb{T}_s and \mathbb{T}_h the BC-expanded and tested counterparts of the discretized operators \mathbf{T} , \mathbf{T}_s and \mathbf{T}_h computed with the complex wavenumber $-jk$.

The solutions of (8) and (9) can be expressed as linear combinations of divergence free (loop and harmonic functions) and of non-divergence free (star functions) contributions via a quasi-Helmholtz decomposition

$$\mathbf{j} = \mathbf{A} \mathbf{l} + \mathbf{\Sigma} \mathbf{s} + \mathbf{H} \mathbf{h} \quad (17)$$

where the first two matrices $\mathbf{A} \in \mathbb{R}^{N_e \times N_v}$ and $\mathbf{\Sigma} \in \mathbb{R}^{N_e \times N_f}$ represent mappings from the RWG subspace to the local loop and star subspaces, respectively. Here, N_v and N_f are the number of vertices and facets of the mesh, respectively [12],

[46]. These two mappings can be defined using only the connectivity information of the discretized geometry as

$$\Lambda_{ij} = \begin{cases} 1 & \text{if node } j \text{ equals } v_i^+ \\ -1 & \text{if node } j \text{ equals } v_i^- \\ 0 & \text{otherwise} \end{cases} \quad (18)$$

and

$$\Sigma_{ij} = \begin{cases} 1 & \text{if the cell } j \text{ equals } c_i^+ \\ -1 & \text{if the cell } j \text{ equals } c_i^- \\ 0 & \text{otherwise,} \end{cases} \quad (19)$$

where vertices v_i^- and v_i^+ define the oriented edge characterizing RWG function i , and c_i^- and c_i^+ denote the corresponding cells (Figure 1). The matrix \mathbf{H} represents the mapping from the RWG space to the quasi-harmonic or *global loop* space composed of $2N_h$ functions, where N_h is the number of handles in the structure. For a complete description of this mapping and the associated harmonic functions, the reader is referred to [12] and [46].

A few properties of these matrices are recalled next to facilitate further developments. For the sake of simplicity we restrict ourselves to the case of a geometry with a single closed connected component. All derivations below can be extended to arbitrary geometries using the relations in [47]. Given this assumption, Λ has a null-space spanned by the all-one vector $\mathbf{1}^\Lambda \in \mathbb{R}^{N_v}$, i.e.

$$\Lambda \mathbf{1}^\Lambda = \mathbf{0}. \quad (20)$$

Similarly, linear dependency of the star functions cause Σ to exhibit a one-dimensional null-space spanned by the all-one vector $\mathbf{1}^\Sigma \in \mathbb{R}^{N_f}$, i.e.

$$\Sigma \mathbf{1}^\Sigma = \mathbf{0}. \quad (21)$$

Finally, it is trivial to show that the loop and star subspaces are orthogonal, i.e.

$$\Sigma^T \Lambda = \mathbf{0}. \quad (22)$$

As Λ and Σ are ill-conditioned and because of the high computational cost of detecting global loops required to build \mathbf{H} , it is convenient to leverage the quasi-Helmholtz projectors introduced in [37] to obtain a quasi-Helmholtz decomposition of the EFIE and MFIE operators. The projectors are defined as

$$\mathbf{P}^\Sigma = \Sigma (\Sigma^T \Sigma)^+ \Sigma^T, \quad (23)$$

$$\mathbf{P}^{\Lambda H} = \mathbf{I} - \mathbf{P}^\Sigma, \quad (24)$$

where $^+$ denotes the Moore-Penrose pseudo-inverse and \mathbf{I} is the identity. Any RWG expansion coefficient vector can then be decomposed as

$$\mathbf{j} = (\mathbf{P}^{\Lambda H} \mathbf{j}) + (\mathbf{P}^\Sigma \mathbf{j}) \quad (25)$$

where $\mathbf{P}^{\Lambda H} \mathbf{j}$ and $\mathbf{P}^\Sigma \mathbf{j}$ contain the RWG expansions of the solenoidal (loop) and non-solenoidal (star) components of the current, respectively. These operators are self-adjoint and also

can be used to decompose the RWG testing space. Similarly, the dual projectors \mathbb{P}^Λ and $\mathbb{P}^{\Sigma H}$, defined as

$$\mathbb{P}^\Lambda = \Lambda (\Lambda^T \Lambda)^+ \Lambda^T, \quad (26)$$

$$\mathbb{P}^{\Sigma H} = \mathbf{I} - \mathbb{P}^\Lambda, \quad (27)$$

decompose any linear combination of BC (basis or testing) functions into a non-solenoidal and solenoidal part, respectively. It should be noted that construction of these projectors does not require the detection of global loops, and that $(\Sigma^T \Sigma)^+$ can be efficiently computed using multigrid preconditioners [37], [48].

III. REGULARIZING THE MFIE AT EXTREMELY LOW FREQUENCIES

A. Low Frequency Behaviour of the MFIE

The standard RWG discretization of the MFIE fails to provide accurate results at low frequencies due to the unphysical scaling of the loop and star (or tree) components of the current [4]. It was shown in [3], [49] that the mixed discretization of the MFIE (in which BC or CW functions [50] are used as testing functions) improves accuracy. In particular, the loop and star components of the current obtained from this formulation scale physically [32]. This result also holds true for multiply connected geometries [51].

The mixed MFIE formulation still suffers from three problems. First, the physical scaling of the current can only be retrieved when interaction integrals are computed to high accuracy [32]. Second, the nonsolenoidal current component scales as $\mathcal{O}(\omega)$ whereas the solenoidal component is of $\mathcal{O}(1)$. As a result, at very low frequencies and when using finite precision, both components should be stored in different arrays to prevent the nonsolenoidal component from losing accuracy or even being cancelled out [4], [5], [31], [51], [52]. Third, the static MFIE (at $\omega = 0$) has a null space when applied to multiply connected geometries. It follows that the discretized MFIE has N_h singular values that scale as $\mathcal{O}(\omega^2)$ [46]. Any accurate discretization of the MFIE operator must preserve this null-space. Standard RWG discretizations of the MFIE operators are not capable of correctly modelling this null space [43]. The mixed MFIE, on the other hand, correctly models this-null space in infinite precision. However, after discretization, the null-space associated singular values will not be more accurate than the precision of the quadrature rule.

B. A Robust MFIE Formulation

To address the above described MFIE deficiencies we propose the following symmetrized MFIE:

$$\left(\frac{\mathcal{I}}{2} - \mathcal{K}_{-jk} \right) \left(\frac{\mathcal{I}}{2} + \mathcal{K}_k \right) (\mathbf{j}) = \left(\frac{\mathcal{I}}{2} - \mathcal{K}_{-jk} \right) (\hat{\mathbf{n}}_r \times \mathbf{h}^i). \quad (28)$$

This equation is the magnetic field counterpart of the (localized) Calderón preconditioned electric operator in [37]. We propose to discretize (28) as

$$\begin{aligned} & \mathbb{M}^T \left(\frac{\mathbf{G}^T}{2} - \mathbf{K}_{-jk} \right) (\mathbf{G}^T)^{-1} \left(\frac{\mathbf{G}^T}{2} + \mathbf{K}_k \right) \mathbf{M} \mathbf{i} \\ & = \mathbf{O} \mathbf{i} = \mathbb{M}^T \left(\frac{\mathbf{G}^T}{2} - \mathbf{K}_{-jk} \right) (\mathbf{G}^T)^{-1} \mathbf{v}_h \end{aligned} \quad (29)$$

where

$$\mathbf{M} = \mathbf{P}^{\Lambda H} \frac{1}{\alpha} + \mathbf{j} \mathbf{P}^{\Sigma} \alpha, \quad (30)$$

$$\mathbb{M} = \mathbb{P}^{\Sigma H} \frac{1}{\alpha} + \mathbf{j} \mathbb{P}^{\Lambda}, \quad (31)$$

and $\mathbf{M} \mathbf{i} = \mathbf{j}$.

The coefficient α allows for re-scaling of the loop and star components of the solution \mathbf{i} of (29) to prevent numerical cancellations. Because $\mathbf{P}^{\Sigma} + \mathbf{P}^{\Lambda H} = \mathbb{P}^{\Lambda} + \mathbb{P}^{\Sigma H} = \mathbf{I}$, operator \mathbf{O} in (29) can be decomposed as

$$\mathbf{O} = (\mathbb{P}^{\Lambda} + \mathbb{P}^{\Sigma H}) \mathbf{O} (\mathbf{P}^{\Sigma} + \mathbf{P}^{\Lambda H}) = \mathbb{P}^{\Lambda} \mathbf{O} \mathbf{P}^{\Sigma} + \mathbb{P}^{\Lambda} \mathbf{O} \mathbf{P}^{\Lambda H} + \mathbb{P}^{\Sigma H} \mathbf{O} \mathbf{P}^{\Sigma} + \mathbb{P}^{\Sigma H} \mathbf{O} \mathbf{P}^{\Lambda H}, \quad (32)$$

which allows for the study of the low-frequency behavior of each of the separate terms. Analysis of the frequency behavior of the first three terms is quite straightforward and yields

$$\mathbb{P}^{\Lambda} \mathbf{O} \mathbf{P}^{\Sigma} = \mathcal{O}(\alpha^2) \quad k \rightarrow 0, \quad (33a)$$

$$\mathbb{P}^{\Lambda} \mathbf{O} \mathbf{P}^{\Lambda H} = \mathcal{O}(1) \quad k \rightarrow 0, \quad (33b)$$

$$\mathbb{P}^{\Sigma H} \mathbf{O} \mathbf{P}^{\Sigma} = \mathcal{O}(1) \quad k \rightarrow 0. \quad (33c)$$

Analysis of the last term in (32) requires special care. It is known that when decomposing \mathbf{K}_k as

$$\mathbf{K}_k = \mathbf{K}_0 + \mathbf{K}'_k, \quad (34)$$

where \mathbf{K}_0 is the static limit of \mathbf{K}_k and $\mathbf{K}'_k = \mathbf{K}_k - \mathbf{K}_0$ is the dynamic remainder, $\mathbf{K}'_k = \mathcal{O}(k^2)$ as $k \rightarrow 0$ [51]. When using this decomposition in (29), it can be verified that \mathbf{K}_0 satisfies

$$\mathbb{P}^{\Sigma H} \left(\frac{\mathbf{G}^T}{2} - \mathbf{K}_0 \right) (\mathbf{G}^T)^{-1} \left(\frac{\mathbf{G}^T}{2} + \mathbf{K}_0 \right) \mathbf{P}^{\Lambda H} = \mathbf{0}. \quad (35)$$

The above equation holds the key to unlocking a frequency-stable MFIE. The proof of property (35) is provided in Appendix A. The term $\mathbb{P}^{\Sigma H} \mathbf{O} \mathbf{P}^{\Lambda H}$ can now be studied. To this end, note that

$$\begin{aligned} & \alpha^2 \mathbb{P}^{\Sigma H} \mathbf{O} \mathbf{P}^{\Lambda H} = \\ &= \mathbb{P}^{\Sigma H} \left(\frac{\mathbf{G}^T}{2} - \mathbf{K}_0 \right) (\mathbf{G}^T)^{-1} \left(\frac{\mathbf{G}^T}{2} + \mathbf{K}_0 \right) \mathbf{P}^{\Lambda H} \\ &+ \mathbb{P}^{\Sigma H} \left(\frac{\mathbf{G}^T}{2} - \mathbf{K}_0 \right) (\mathbf{G}^T)^{-1} (\mathbf{K}'_k) \mathbf{P}^{\Lambda H} \\ &- \mathbb{P}^{\Sigma H} (\mathbf{K}'_{-jk}) (\mathbf{G}^T)^{-1} \left(\frac{\mathbf{G}^T}{2} + \mathbf{K}_0 \right) \mathbf{P}^{\Lambda H} \\ &- \mathbb{P}^{\Sigma H} (\mathbf{K}'_{-jk}) (\mathbf{G}^T)^{-1} (\mathbf{K}'_k) \mathbf{P}^{\Lambda H} \\ &= 0 + \mathcal{O}(k^2) + \mathcal{O}(k^2) - \mathcal{O}(k^4), \end{aligned} \quad (36)$$

which completes the low-frequency analysis of the overall operator

$$\begin{aligned} \mathbf{O} &= \mathbb{P}^{\Lambda} \mathbf{O} \mathbf{P}^{\Sigma} + \mathbb{P}^{\Lambda} \mathbf{O} \mathbf{P}^{\Lambda H} + \mathbb{P}^{\Sigma H} \mathbf{O} \mathbf{P}^{\Sigma} + \mathbb{P}^{\Sigma H} \mathbf{O} \mathbf{P}^{\Lambda H} \\ &= \mathcal{O}(\alpha^2) + \mathcal{O}(1) + \mathcal{O}(1) + \mathcal{O}\left(\frac{k^2}{\alpha^2}\right). \end{aligned} \quad (37)$$

To choose α , in addition to the conditioning constraint imposed by (37), we need to consider the physical scaling of the current, which for a plane wave excitation, is [5]

$$\mathbf{P}^{\Lambda H} \mathbf{j} = \mathcal{O}(1), \quad (38)$$

$$\mathbf{P}^{\Sigma} \mathbf{j} = \mathcal{O}(k). \quad (39)$$

These scaling laws reveal that for a standard formulation, a severe numerical cancellation is expected due to the fact that the non-solenoidal component of the current (which scales as $\mathcal{O}(k)$) will disappear when stored alongside the solenoidal component (which scales as $\mathcal{O}(1)$). Instead, for the regularized formulation proposed here, the equation is solved for $\mathbf{i} = \mathbf{M}^{-1} \mathbf{j}$, which scales as

$$\mathbf{P}^{\Lambda H} \mathbf{i} = \mathcal{O}(\alpha), \quad (40)$$

$$\mathbf{P}^{\Sigma} \mathbf{i} = \mathcal{O}(k/\alpha). \quad (41)$$

It is now evident that by setting $\alpha = \sqrt{k}$, the above scaling behaviors become

$$\mathbf{P}^{\Lambda H} \mathbf{i} = \mathcal{O}(\sqrt{k}), \quad (42)$$

$$\mathbf{P}^{\Sigma} \mathbf{i} = \mathcal{O}(\sqrt{k}), \quad (43)$$

eliminating the low frequency cancellation and, at the same time, stabilizing the matrix at low frequencies. The latter is seen upon inserting the new scalings into (37):

$$\begin{aligned} \mathbf{O} &= \mathcal{O}(\alpha^2) + \mathcal{O}(1) + \mathcal{O}(1) + \mathcal{O}\left(\frac{k^2}{\alpha^2}\right) \\ &= \mathcal{O}(k) + \mathcal{O}(1) + \mathcal{O}(1) + \mathcal{O}(k). \end{aligned} \quad (44)$$

The deficiency of the MFIE in the static regime also is solved by the scheme proposed here. In fact, using (37) when $k = 0$ we obtain

$$\mathbf{O} \mathbf{P}^{\Lambda H} = \mathbb{P}^{\Lambda} \mathbf{O} \mathbf{P}^{\Lambda H}, \quad (45)$$

which proves the existence of an exact matrix null-space in statics of dimension exactly equal to that of the harmonic subspace.

Summarizing, the proposed MFIE resolves the three main issues of prior standard and non-standard MFIE formulations and now can be linearly combined with EFIEs using projectors.

IV. A NEW CFIE

The theoretical developments of the previous sections resulted in a magnetic field operator that can be stably discretized for arbitrarily low frequencies using standard integration rules. The electric counterpart of this operator was obtained in [37]. We will now combine these two operators, first proving the resonance-free property of their continuous combination at high frequencies, and then showing their compatibility at arbitrarily low frequencies.

Standard Calderón CFIE equations use a localization strategy for the EFIE component to obtain a resonance-free equation [22], [23]. Here, we follow the Yukawa-Calderón approach in [22]. When the Yukawa-Calderón EFIE is linearly combined with the new magnetic operator defined in Section III, the following symmetric Yukawa-Calderón CFIE is obtained:

$$\begin{aligned} & \left(\eta^2 \left(\frac{\mathcal{I}}{2} - \mathcal{K}_{-jk} \right) \left(\frac{\mathcal{I}}{2} + \mathcal{K}_k \right) (k) + \mathcal{T}_{-jk} \mathcal{T}_k \right) (j) = \\ & \left(\frac{\mathcal{I}}{2} - \mathcal{K}_{-jk} \right) (\hat{\mathbf{n}} \times \mathbf{h}^i) + \mathcal{T}_{-jk} (\hat{\mathbf{n}} \times \mathbf{e}^i). \end{aligned} \quad (46)$$

To demonstrate that this equation represents a valid Calderón CFIE, i.e. is free from internal resonances, we prove in Appendix B that the operator

$$\left(\eta^2 \left(\frac{\mathcal{I}}{2} - \mathcal{K}_{-jk} \right) \left(\frac{\mathcal{I}}{2} + \mathcal{K}_k \right) (k) + \mathcal{T}_{-jk} \mathcal{T}_k \right) \quad (47)$$

can be inverted for any k .

The discretization of the proposed Yukawa-Calderón CFIE follows directly from that of the new MFIE in Section III and that of the EFIE in [37]:

$$\begin{aligned} & \eta^2 M^T \left(\frac{\mathbf{G}^T}{2} - \mathbf{K}_{-jk} \right) (\mathbf{G}^T)^{-1} \left(\frac{\mathbf{G}^T}{2} + \mathbf{K}_k \right) \mathbf{M} \mathbf{i} \\ & + M^T T M (\mathbf{G})^{-1} M^T T M \mathbf{i} \\ = & \eta^2 M^T \left(\frac{\mathbf{G}^T}{2} - \mathbf{K}_{-jk} \right) (\mathbf{G}^T)^{-1} \mathbf{v}_h \\ & + M^T T M (\mathbf{G})^{-1} M^T \mathbf{v}_e. \end{aligned} \quad (48)$$

Here $\alpha = 1$ and $\alpha = \sqrt{k}$ in the high and low frequency regime, respectively. We next study the latter more in detail.

Scaling in the latter regime follows from the results of the previous section:

$$\begin{aligned} & \eta^2 M^T \left(\frac{\mathbf{G}^T}{2} - \mathbf{K}_{-jk} \right) (\mathbf{G}^T)^{-1} \left(\frac{\mathbf{G}^T}{2} + \mathbf{K}_k \right) \mathbf{M} \mathbf{i} \\ & + M^T T M (\mathbf{G})^{-1} M^T T M \mathbf{i} \\ = & -j \left(P^{\Sigma H} T_s P^{\Sigma H} \right) \mathbf{G}^{-1} T_h + j T_h \mathbf{G}^{-1} (P^{AH} T_s P^{AH}) + \\ & j \left(P^{\Sigma H} T_s P^{\Sigma H} \right) \mathbf{G}^{-1} (P^{AH} T_s P^{AH}) + \\ & \eta^2 P^{\Sigma H} \left(\frac{\mathbf{G}^T}{2} - \mathbf{K}_0 \right) (\mathbf{G}^T)^{-1} \left(\frac{\mathbf{G}^T}{2} + \mathbf{K}_0 \right) j P^{\Sigma} + \\ & \eta^2 j P^A \left(\frac{\mathbf{G}^T}{2} - \mathbf{K}_0 \right) (\mathbf{G}^T)^{-1} \left(\frac{\mathbf{G}^T}{2} + \mathbf{K}_0 \right) P^{AH} + \\ & \mathcal{O}(k) \\ = & \mathcal{O}(1) + \mathcal{O}(1) + \mathcal{O}(1) + \mathcal{O}(1) + \mathcal{O}(1) + \mathcal{O}(k). \end{aligned} \quad (49)$$

Combining this result with the corresponding right hand side scalings (42) and (43) proves the overall low-frequency stability of new CFIE.

V. NUMERICAL RESULTS

This section presents numerical results that validate the above properties of the proposed MFIE and CFIE.

The first set of tests involve a PEC sphere of radius 1 m. Figure 2 shows the scattered far field at $f = 200$ MHz obtained using the new MFIE and CFIE as well as other established formulations (standard EFIE, EFIE with projectors, Calderón EFIE with projectors, Mixed MFIE, CFIE). For this high frequency case all formulations deliver accurate results, thus validating our implementations. A first difference in performance between our new formulations and their standard counterparts is noted when lowering the frequency. Figure 3 shows data similar to Figure 2 but for $f = 1 \times 10^{-40}$ Hz. It is clear that accuracy breakdowns occur for the non-projected methods – the mixed MFIE, the EFIE, and the CFIE (for the latter two the lack of accuracy also is due to conditioning problems). On the other hand, all projected formulations, including

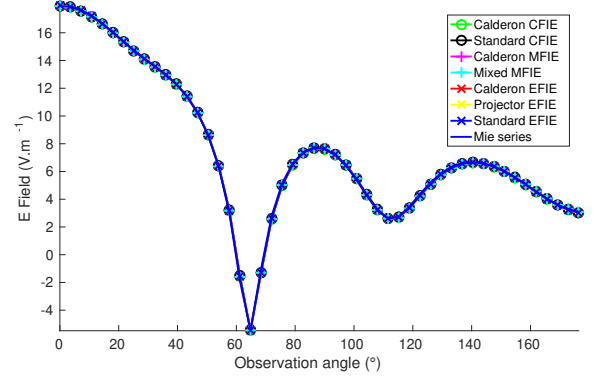


Figure 2. Comparison of the far field scattered by a PEC sphere of radius 1 m discretized with an average edge size of 0.15 m and excited by a plane wave oscillating at 200 MHz.

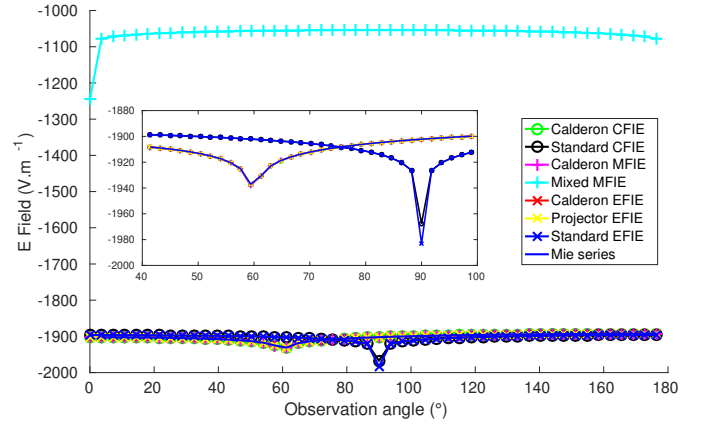


Figure 3. Comparison of the far field scattered by a PEC sphere of radius 1 m discretized with an average edge size of 0.15 m and excited by a plane wave oscillating at 1×10^{-40} Hz.

the two new ones, deliver accurate results for arbitrarily low frequencies.

The low frequency stability of the new Calderón MFIE is further demonstrated in Figure 4, which illustrates the conditioning of the different operators for low frequencies. It is clear that the new MFIE remains as well-conditioned as its standard counterpart. The Calderón CFIE is also low-frequency stable, unlike the standard CFIE, which exhibits a severe ill-conditioning caused by its EFIE contribution.

Figure 5 shows that, despite its regularized low frequency behavior, the Calderón MFIE is prone to spurious resonances causing it to become periodically ill-conditioned. This issue is shared by all non-combined formulations and can be overcome by combined field strategies. It is clear from the figure that both the new Calderón CFIE and its standard counterpart exhibit resonance-free behaviour.

The last key property to be illustrated is the refinement stability of the proposed formulations. This property was verified by studying the dependence of the condition number of the different formulations applied to a unit radius sphere with increasing discretization density (Figure 6). These results confirm that the second kind nature of our new formulations renders them immune to the high-refinement breakdown.

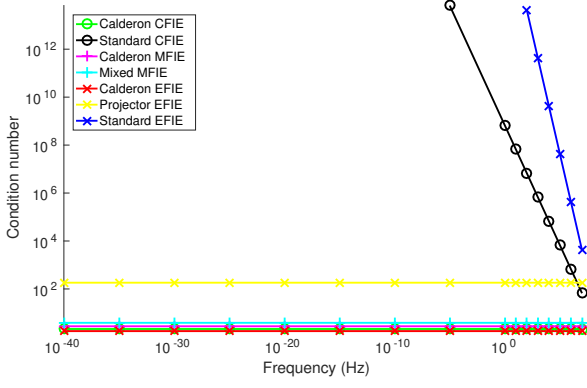


Figure 4. Low frequency behaviour of the conditioning of the different operators on a PEC sphere of radius 1 m. Because of numerical limitations in the computation of very high condition numbers ($> 1 \times 10^{16}$) some points have been left out.

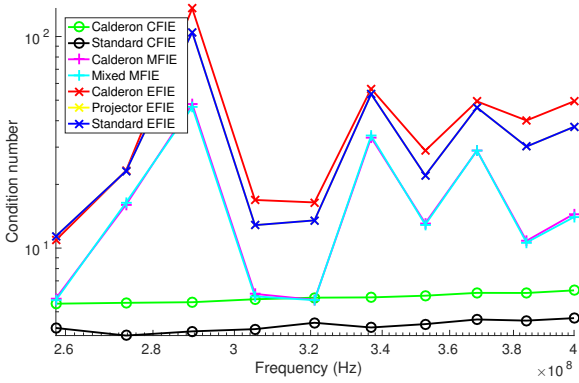


Figure 5. High frequency behaviour of the conditioning of the different operators on a PEC sphere of radius 1 m sphere illustrating the spurious resonances occurring in non-combined formulations. The average edge size of the discretized sphere has been kept at one-fifth of the wavelength for every simulation.

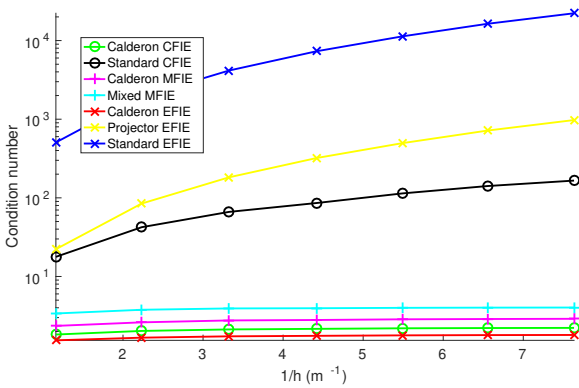


Figure 6. High-refinement behaviour of the conditioning of the different operators on a PEC sphere of radius 1 m. The non-resonant frequency has been kept constant for all simulations and corresponds to 5 unknowns per wavelength discretization for the least refined point.

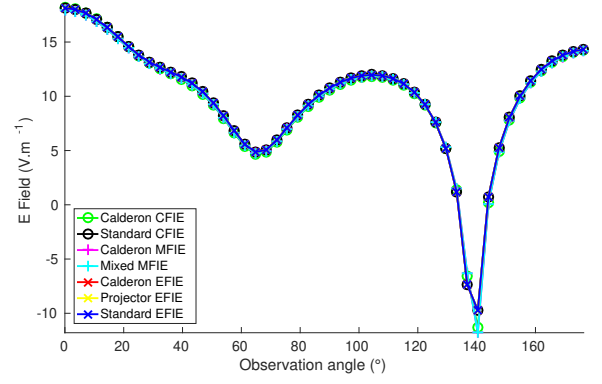


Figure 7. Comparison of the far field scattered by a PEC square torus with an inner radius of 0.5 m and a tube radius of 0.25 m, discretized with an average edge size of 0.15 m and excited by a plane wave oscillating at 200 MHz.

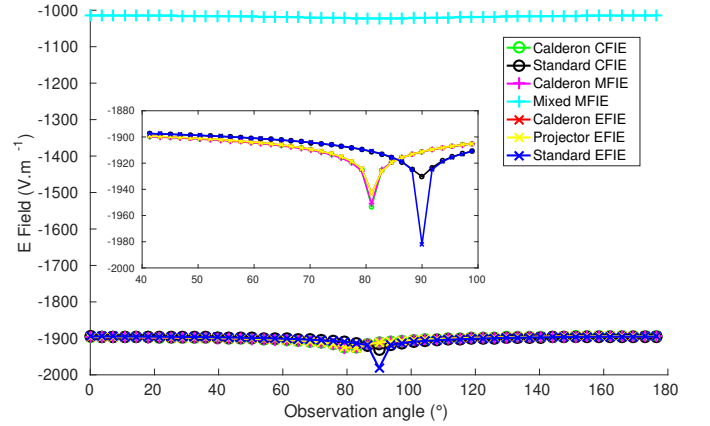


Figure 8. Comparison of the far field scattered by a PEC square torus with an inner radius of 0.5 m and a tube radius of 0.25 m, discretized with an average edge size of 0.15 m and excited by a plane wave oscillating at 1×10^{-40} Hz.

In summary, the above results show that the new Calderón MFIE yields correct results for arbitrarily low frequencies and is well conditioned for both low frequencies and dense discretization. Additionally, when combined with the projector Calderón EFIE the new Calderón CFIE, which is low frequency stable, immune to dense discretization breakdown, and free from non-physical resonances, is obtained.

To ensure that the properties illustrated so far still persist for multiply connected structures, many of the previous analyses were repeated for a square torus. The correctness of the formulation has been verified by studying the far field scattered by the torus at high and very low frequencies, respectively (Figures 7 and 8). Since no analytic solution is readily available for the square torus, the solution of the Calderón EFIE was used as a reference and particular care was taken to avoid frequencies corresponding to an internal resonance. While the results are similar to those of the sphere, the reader should be aware that, because of its toroidal and poloidal null-spaces, the Calderón MFIE required the usage of a pseudo inversion to obtain current solutions at very low frequencies.

The low frequency stability of the Calderón MFIE and Calderón CFIE on the toroidal structure are demonstrated in Figure 9, while their resonance free behaviors are illustrated in

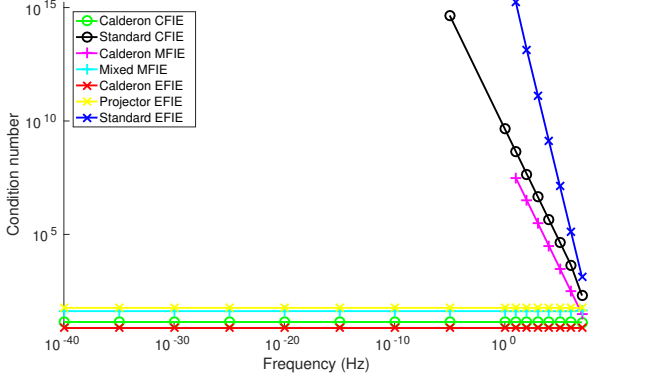


Figure 9. Low frequency behaviour of the conditioning of the different operators on a PEC square torus with an inner radius of 0.5 m, a tube radius of 0.25 m and meshed with an average edge length of 0.6 m. Because of numerical limitations in the computation of very high condition numbers ($> 1 \times 10^{16}$) some points have been left out.

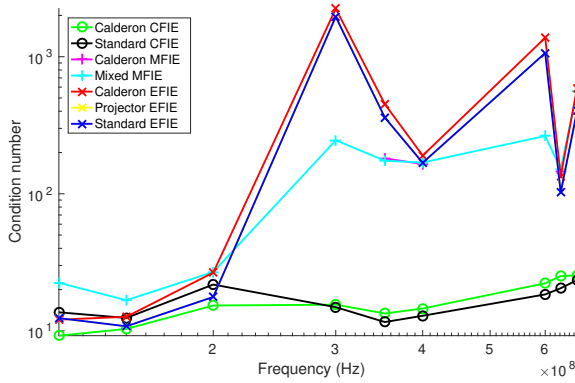


Figure 10. High frequency behaviour of the conditioning of the different operators on a PEC square torus of inner radius of 0.5 m and tube radius of 0.25 m, illustrating the resonances of non-combined formulations. The average edge size of the discretization has been kept at one-fifth of the wavelength for every simulation.

Figure 10. Finally, the resilience of both formulations to dense discretization breakdown is illustrated in Figure 11, which presents the condition number of the integral operators with increasing discretization of the square torus.

One of the key advantages of the new Calderón MFIE scheme is that it does not require extremely accurate numerical integration rules because it allows explicit cancellation of near-zero terms that are challenging to obtain numerically. The slow convergence of the standard numerical integration schemes can be seen in Figure 12, in which the ratio of the norm of the term in (50) to the norm of the full operator with increasing number of integration points is presented. While this ratio does decrease with the number of Gaussian quadrature points, it does so very slowly and remains far from a machine-precision zero value. The effect of these numerical inaccuracies is evident when comparing the singular value decompositions of the Mixed MFIE and of the new Calderón MFIE in Figure 13. It is clear that the null singular values corresponding to the toroidal and poloidal subspaces of the square torus immediately reach the machine precision zero in

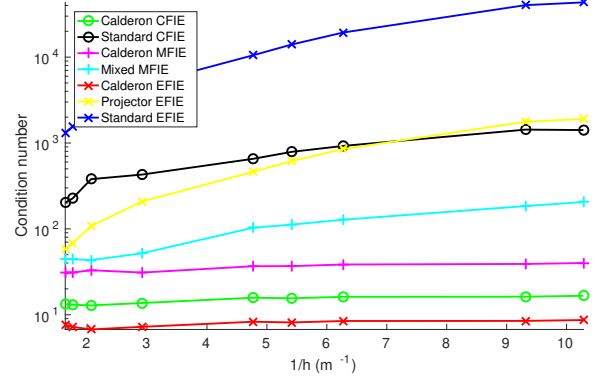


Figure 11. High-refinement behaviour of the conditioning of the different operators on a PEC square torus of inner radius of 0.5 m and tube radius of 0.25 m. The non-resonant frequency has been kept constant for all simulations and corresponds to a 5 unknowns per wavelength discretization for the least refined point.

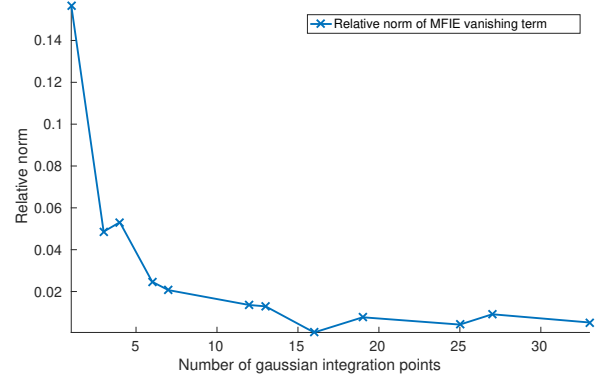


Figure 12. Decay of the relative (with regards to the full operator) norm of cancelled out term (50) of the Calderón CFIE as a function of the number of Gaussian integration points. These results correspond to a square torus of inner radius 0.5 m and tube radius 0.25 m simulated at 1×10^{-10} Hz.

the case of the Calderón MFIE, while for the Mixed MFIE they will require an unreasonably complex integration rules to even remotely resemble a nullspace.

Finally, to demonstrate that our schemes can be readily applied to more complex problems we studied the low frequency conditioning of our operators (Figure 15) for the complex, multiply connected geometry in Figure 14.

VI. CONCLUSION

This paper presented a new symmetrized MFIE that can be stably and effectively discretized using quasi-Helmholtz projectors. When linearly combined with a quasi-Helmholtz projector-based Calderón EFIE, a new CFIE that is immune from all drawbacks that plague the majority of existing formulations is obtained. In fact, the proposed CFIE remains well-conditioned both at low frequencies and for high discretization densities, allows for an accurate solution at extremely low frequencies without requiring special numerical quadrature methods, does not require the detection of global loops when applied to multiply connected geometries, and is provably

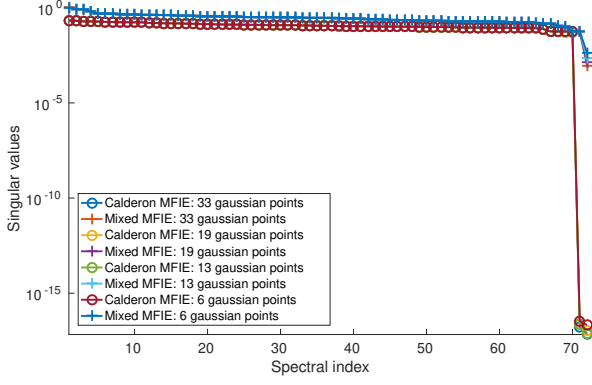


Figure 13. Accuracy of the toroidal and poloidal nullspaces obtained by the Calderón and Mixed MFIE as a function of the number of Gaussian integration points. The results correspond to a square torus of inner radius 0.5 m and tube radius 0.25 m simulated at 1×10^{-10} Hz.

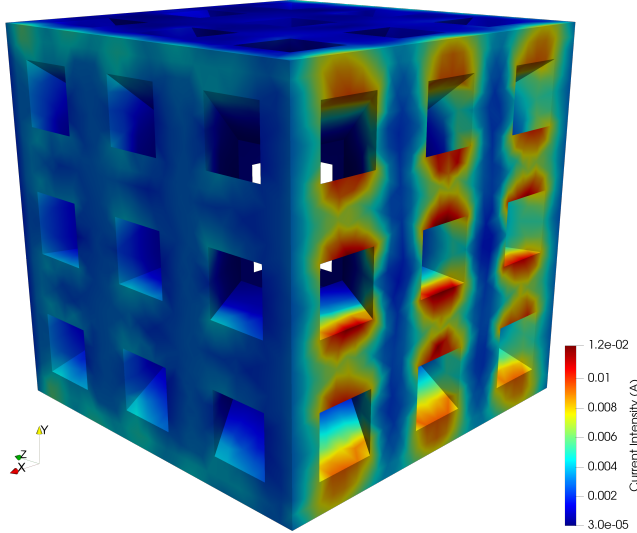


Figure 14. Complex multiply-connected geometry discretized with an average edge length of 0.35 m. The values represented on the geometry correspond to the intensity of the current induced on the PEC structure by a plane wave. The simulating frequency corresponds to 10 unknowns per wavelength.

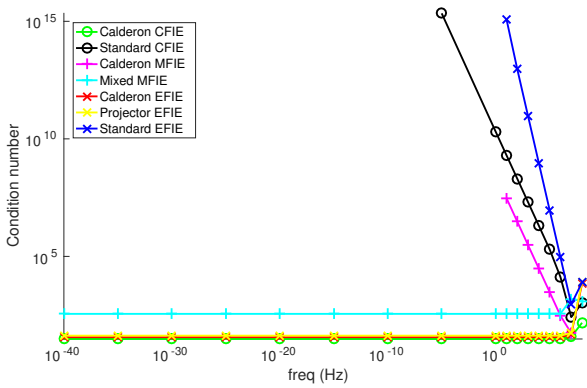


Figure 15. Low frequency behaviour of the conditioning of the different operators on the structure illustrated in Figure 14. Because of numerical limitations in the computation of very high condition numbers ($> 1 \times 10^{16}$) some points have been left out.

free from internal resonances. Numerical results confirm the theoretically predicted properties of the proposed equations.

APPENDIX A

PROOF OF THE FUNDAMENTAL MATRIX RELATIONSHIP (35)

To prove the validity of (35), i.e.

$$\mathbb{P}^{\Sigma H} \left(\frac{\mathbf{G}^T}{2} - \mathbf{K}_0 \right) (\mathbf{G}^T)^{-1} \left(\frac{\mathbf{G}^T}{2} + \mathbf{K}_0 \right) \mathbf{P}^{\Lambda H} = \mathbf{0}, \quad (50)$$

we introduce \mathbf{P}^{Pol} , \mathbf{P}^{Tor} , \mathbb{P}^{Pol} , \mathbb{P}^{Tor} the orthogonal projectors into the right and left null-spaces of the internal and external MFIE operators, i.e.

$$\left(\frac{\mathbf{G}^T}{2} + \mathbf{K}_0 \right) \mathbf{P}^{\text{Pol}} = \mathbf{0}, \quad (51)$$

$$\left(\frac{\mathbf{G}^T}{2} - \mathbf{K}_0 \right) \mathbf{P}^{\text{Tor}} = \mathbf{0}, \quad (52)$$

$$\mathbb{P}^{\text{Pol}} \left(\frac{\mathbf{G}^T}{2} - \mathbf{K}_0 \right) = \mathbf{0}, \quad (53)$$

$$\mathbb{P}^{\text{Tor}} \left(\frac{\mathbf{G}^T}{2} + \mathbf{K}_0 \right) = \mathbf{0}. \quad (54)$$

Note that

$$\left(\frac{\mathbf{G}^T}{2} + \mathbf{K}_0 \right) \mathbf{P}^{\text{Tor}} = \mathbf{G}^T \mathbf{P}^{\text{Tor}}, \quad (55)$$

$$\left(\frac{\mathbf{G}^T}{2} - \mathbf{K}_0 \right) \mathbf{P}^{\text{Pol}} = \mathbf{G}^T \mathbf{P}^{\text{Pol}}, \quad (56)$$

$$\mathbb{P}^{\text{Tor}} \left(\frac{\mathbf{G}^T}{2} - \mathbf{K}_0 \right) = \mathbb{P}^{\text{Tor}} \mathbf{G}^T, \quad (57)$$

$$\mathbb{P}^{\text{Pol}} \left(\frac{\mathbf{G}^T}{2} + \mathbf{K}_0 \right) = \mathbb{P}^{\text{Pol}} \mathbf{G}^T. \quad (58)$$

We can then define

$$\mathbf{Q}^{\Lambda} = \mathbf{P}^{\Lambda H} - \mathbf{P}^{\text{Pol}} - \mathbf{P}^{\text{Tor}}, \quad (59)$$

which clearly satisfies

$$\mathbb{P}^{\Lambda} \mathbf{Q}^{\Lambda} = \mathbf{Q}^{\Lambda}, \quad (60)$$

since the union of the right null spaces of the internal and external MFIE operators contains all the non-trivial cycles of the structure [46]. Dually,

$$\mathbf{Q}^{\Sigma} = \mathbb{P}^{\Sigma H} - \mathbb{P}^{\text{Pol}} - \mathbb{P}^{\text{Tor}}, \quad (61)$$

satisfies

$$\mathbf{P}^{\Sigma} \mathbf{Q}^{\Sigma} = \mathbf{Q}^{\Sigma}. \quad (62)$$

It follows that

$$\begin{aligned}
& \left(\frac{\mathbf{G}^T}{2} - \mathbf{K}_0 \right) (\mathbf{G}^T)^{-1} \left(\frac{\mathbf{G}^T}{2} + \mathbf{K}_0 \right) \mathbf{P}^{\Lambda H} \\
&= \left(\frac{\mathbf{G}^T}{2} - \mathbf{K}_0 \right) (\mathbf{G}^T)^{-1} \left(\frac{\mathbf{G}^T}{2} + \mathbf{K}_0 \right) (\mathbf{Q}^\Lambda + \mathbf{P}^{\text{Pol}} + \mathbf{P}^{\text{Tor}}) \\
&= \left(\frac{\mathbf{G}^T}{2} - \mathbf{K}_0 \right) (\mathbf{G}^T)^{-1} \left(\frac{\mathbf{G}^T}{2} + \mathbf{K}_0 \right) \mathbf{Q}^\Lambda \\
&+ \left(\frac{\mathbf{G}^T}{2} - \mathbf{K}_0 \right) (\mathbf{G}^T)^{-1} \left(\frac{\mathbf{G}^T}{2} + \mathbf{K}_0 \right) \mathbf{P}^{\text{Tor}} \\
&= \left(\frac{\mathbf{G}^T}{2} - \mathbf{K}_0 \right) (\mathbf{G}^T)^{-1} \left(\frac{\mathbf{G}^T}{2} + \mathbf{K}_0 \right) \mathbf{Q}^\Lambda \\
&+ \left(\frac{\mathbf{G}^T}{2} - \mathbf{K}_0 \right) \mathbf{P}^{\text{Tor}} \\
&= \left(\frac{\mathbf{G}^T}{2} - \mathbf{K}_0 \right) (\mathbf{G}^T)^{-1} \left(\frac{\mathbf{G}^T}{2} + \mathbf{K}_0 \right) \mathbf{Q}^\Lambda,
\end{aligned} \tag{63}$$

and similarly that

$$\begin{aligned}
& \mathbb{P}^{\Sigma H} \left(\frac{\mathbf{G}^T}{2} - \mathbf{K}_0 \right) (\mathbf{G}^T)^{-1} \left(\frac{\mathbf{G}^T}{2} + \mathbf{K}_0 \right) \\
&= \mathbf{Q}^\Sigma \left(\frac{\mathbf{G}^T}{2} - \mathbf{K}_0 \right) (\mathbf{G}^T)^{-1} \left(\frac{\mathbf{G}^T}{2} + \mathbf{K}_0 \right).
\end{aligned} \tag{64}$$

Combining the above equations it follows that

$$\begin{aligned}
& \mathbb{P}^{\Sigma H} \left(\frac{\mathbf{G}^T}{2} - \mathbf{K}_0 \right) (\mathbf{G}^T)^{-1} \left(\frac{\mathbf{G}^T}{2} + \mathbf{K}_0 \right) \mathbf{P}^{\Lambda H} \\
&= \mathbf{Q}^\Sigma \left(\frac{\mathbf{G}^T}{2} - \mathbf{K}_0 \right) (\mathbf{G}^T)^{-1} \left(\frac{\mathbf{G}^T}{2} + \mathbf{K}_0 \right) \mathbf{Q}^\Lambda.
\end{aligned} \tag{65}$$

In the above expression we now insert the identity matrices $(\mathbf{P}^{\Lambda H} + \mathbf{P}^\Sigma)$ and $(\mathbb{P}^{\Sigma H} + \mathbb{P}^\Lambda)$ obtaining

$$\begin{aligned}
(65) &= \mathbf{Q}^\Sigma \left(\frac{\mathbf{G}^T}{2} - \mathbf{K}_0 \right) (\mathbf{P}^{\Lambda H} + \mathbf{P}^\Sigma) (\mathbf{G}^T)^{-1} \\
& \quad (\mathbb{P}^{\Sigma H} + \mathbb{P}^\Lambda) \left(\frac{\mathbf{G}^T}{2} + \mathbf{K}_0 \right) \mathbf{Q}^\Lambda.
\end{aligned} \tag{66}$$

Given that

$$\mathbf{Q}^\Sigma \left(\frac{\mathbf{G}^T}{2} - \mathbf{K}_0 \right) \mathbf{P}^{\Lambda H} = \mathbf{Q}^\Sigma \mathbf{P}^\Sigma \left(\frac{\mathbf{G}^T}{2} - \mathbf{K}_0 \right) \mathbf{P}^{\Lambda H} = \mathbf{0} \tag{67}$$

and that

$$\mathbb{P}^{\Sigma H} \left(\frac{\mathbf{G}^T}{2} + \mathbf{K}_0 \right) \mathbf{Q}^\Lambda = \mathbb{P}^{\Sigma H} \left(\frac{\mathbf{G}^T}{2} + \mathbf{K}_0 \right) \mathbb{P}^\Lambda \mathbf{Q}^\Lambda = \mathbf{0} \tag{68}$$

and considering the property

$$\mathbf{P}^\Sigma (\mathbf{G}^T)^{-1} \mathbb{P}^\Lambda = \mathbf{0}, \tag{69}$$

we obtain that

$$\begin{aligned}
(65) &= \mathbf{P}^\Sigma \left(\frac{\mathbf{G}^T}{2} - \mathbf{K}_0 \right) \mathbf{P}^\Sigma (\mathbf{G}^T)^{-1} \mathbb{P}^\Lambda \left(\frac{\mathbf{G}^T}{2} + \mathbf{K}_0 \right) \mathbb{P}^\Lambda \\
&= \mathbf{0},
\end{aligned} \tag{70}$$

which completes the proof.

APPENDIX B

RESONANCE-FREE PROOF FOR THE NEW CALDERÓN CFIE OPERATOR

Since the operator $\left(\frac{\mathcal{I}}{2} - \mathcal{K} \right) (-jk)$ always admits an inverse, the invertibility of (47) is equivalent to the invertibility of

$$\left(\frac{\mathcal{I}}{2} + \mathcal{K}_k \right) + \left(\frac{\mathcal{I}}{2} - \mathcal{K}_{-jk} \right)^{-1} \mathcal{T}_{-jk} \mathcal{T}_k. \tag{71}$$

Given the anti-commutation property

$$\mathcal{T}^{-1} \mathcal{K} + \mathcal{K} \mathcal{T}^{-1} = 0, \tag{72}$$

which follows directly from the second Calderón identity $\mathcal{T}^{-1} \mathcal{K} = \mathcal{T}^{-1} \mathcal{K} \mathcal{T} \mathcal{T}^{-1} = -\mathcal{T}^{-1} \mathcal{T} \mathcal{K} \mathcal{T}^{-1} = -\mathcal{K} \mathcal{T}^{-1}$, and defining

$$\mathcal{A} = \left(\frac{\mathcal{I}}{2} - \mathcal{K}_{-jk} \right)^{-1} \mathcal{T}_{-jk}, \tag{73}$$

it follows that

$$\begin{aligned}
(\hat{n} \times \mathcal{A})^T &= \left(\hat{n} \times \left(\frac{\mathcal{I}}{2} - \mathcal{K}_{-jk} \right)^{-1} \mathcal{T}_{-jk} \right)^T \\
&= \left(\hat{n} \times \left(\mathcal{T}_{-jk}^{-1} \left(\frac{\mathcal{I}}{2} - \mathcal{K}_{-jk} \right) \right)^{-1} \right)^T \\
&= \left(\hat{n} \times \left(\left(\frac{\mathcal{I}}{2} + \mathcal{K}_{-jk} \right) \mathcal{T}_{-jk}^{-1} \right)^{-1} \right)^T \\
&= \left(\hat{n} \times \mathcal{T}_{-jk} \left(\frac{\mathcal{I}}{2} + \mathcal{K}_{-jk} \right)^{-1} \right)^T \\
&= \left(\left(\frac{\mathcal{I}}{2} + \mathcal{K}_{-jk} \right)^{-1} \right)^T \hat{n} \times \mathcal{T}_{-jk} \\
&= -\hat{n} \times \left(\frac{\mathcal{I}}{2} - \mathcal{K}_{-jk} \right)^{-1} \hat{n} \times \hat{n} \times \mathcal{T}_{-jk} \\
&= \hat{n} \times \left(\frac{\mathcal{I}}{2} - \mathcal{K}_{-jk} \right)^{-1} \mathcal{T}_{-jk} \\
&= \hat{n} \times \mathcal{A}.
\end{aligned} \tag{74}$$

Given this result and the fact that

$$\hat{n} \times \mathcal{A} = \hat{n} \times \left(\frac{\mathcal{I}}{2} - \mathcal{K}_{-jk} \right)^{-1} \mathcal{T}_{-jk} \tag{75}$$

is a real operator, the symmetry implies it being Hermitian, so that

$$\mathbf{x}^\dagger \left(\hat{n} \times \left(\left(\frac{\mathcal{I}}{2} - \mathcal{K}_{-jk} \right) (jk) \right)^{-1} \mathcal{T}_{-jk} \right) \mathbf{x} \tag{76}$$

is real and nonzero. By leveraging a straightforward extension of Theorem 3.1 in [53], it follows that

$$\left(\left(\frac{\mathcal{I}}{2} - \mathcal{K}_{-jk} \right) \left(\frac{\mathcal{I}}{2} + \mathcal{K}_k \right) + \mathcal{T}_{-jk} \mathcal{T}_k \right) \tag{77}$$

is always invertible. Otherwise said, the Yukawa-Calderón CFIE we propose is resonance free.

ACKNOWLEDGMENT

This work has been funded in part by the European Research Council (ERC) under the European Union's Horizon 2020 research and innovation program (ERC project 321, grant No. 724846).

REFERENCES

- [1] J. G. Van Bladel, *Electromagnetic Fields*, 2nd ed., ser. IEEE Press series on electromagnetic wave theory. IEEE Press.
- [2] S. Rao, D. Wilton, and A. Glisson, "Electromagnetic scattering by surfaces of arbitrary shape," vol. 30, no. 3, pp. 409–418.
- [3] K. Cools, F. P. Andriulli, D. De Zutter, and E. Michielssen, "Accurate and Conforming Mixed Discretization of the MFIE," vol. 10, pp. 528–531.
- [4] Yunhua Zhang, Tie Jun Cui, Weng Cho Chew, and Jun-Sheng Zhao, "Magnetic field integral equation at very low frequencies," vol. 51, no. 8, pp. 1864–1871.
- [5] Z.-G. Qian and W. C. Chew, "Enhanced A-EFIE With Perturbation Method," vol. 58, no. 10, pp. 3256–3264.
- [6] Z. G. Qian and W. C. Chew, "A quantitative study on the low frequency breakdown of EFIE," vol. 50, no. 5, pp. 1159–1162.
- [7] D. Wilton and A. Glisson, "On improving the electric field integral equation at low frequencies," vol. 24.
- [8] G. Vecchi, "Loop-star decomposition of basis functions in the discretization of the EFIE," vol. 47, no. 2, pp. 339–346.
- [9] J.-S. Zhao and W. C. Chew, "Integral equation solution of Maxwell's equations from zero frequency to microwave frequencies," vol. 48, no. 10, pp. 1635–1645.
- [10] J.-F. Lee, R. Lee, and R. Burkholder, "Loop star basis functions and a robust preconditioner for EFIE scattering problems," vol. 51, no. 8, pp. 1855–1863.
- [11] T. F. Eibert, "Iterative-solver convergence for loop-star and loop-tree decompositions in method-of-moments solutions of the electric-field integral equation," vol. 46, no. 3, pp. 80–85.
- [12] D. Wilton and A. Glisson, "On improving the stability of the electric field integral equation at low frequency," in *Proc. IEEE Antennas and Propagation Soc. National Symp.*, pp. 124–133.
- [13] F. P. Andriulli, A. Tabacco, and G. Vecchi, "Solving the EFIE at Low Frequencies With a Conditioning That Grows Only Logarithmically With the Number of Unknowns," vol. 58, no. 5, pp. 1614–1624.
- [14] F. P. Andriulli, K. Cools, H. Bagci, F. Olyslager, A. Buffa, S. Christiansen, and E. Michielssen, "A Multiplicative Calderon Preconditioner for the Electric Field Integral Equation," vol. 56, no. 8, pp. 2398–2412.
- [15] F. P. Andriulli, "Loop-Star and Loop-Tree Decompositions: Analysis and Efficient Algorithms," vol. 60, no. 5, pp. 2347–2356.
- [16] Z. G. Qian and W. C. Chew, "An augmented electric field integral equation for high-speed interconnect analysis," vol. 50, no. 10, pp. 2658–2662.
- [17] J. Zhu and D. Jiao, "A Rigorous Solution to the Low-Frequency Breakdown in Full-Wave Finite-Element-Based Analysis of General Problems Involving Inhomogeneous Lossless/Lossy Dielectrics and Nonideal Conductors," vol. 59, no. 12, pp. 3294–3306.
- [18] F. Vipiana, G. Vecchi, and P. Pirinoli, "A Multiresolution System of Rao & Wilton & Glisson Functions," vol. 55, no. 3, pp. 924–930.
- [19] F. P. Andriulli, F. Vipiana, and G. Vecchi, "Hierarchical Bases for Nonhierarchical 3-D Triangular Meshes," vol. 56, no. 8, pp. 2288–2297.
- [20] R. Chen, J. Ding, D. Z. Ding, Z. H. Fan, and D. Wang, "A Multiresolution Curvilinear Rao–Wilton–Glisson Basis Function for Fast Analysis of Electromagnetic Scattering," vol. 57, no. 10, pp. 3179–3188.
- [21] S. H. Christiansen and J.-C. Nedelec, "A Preconditioner for the Electric Field Integral Equation Based on Calderon Formulas," vol. 40, no. 3, pp. 1100–1135.
- [22] H. Contopanagos, B. Dembart, M. Epton, J. Ottusch, V. Rokhlin, J. Visser, and S. Wandzura, "Well-conditioned boundary integral equations for three-dimensional electromagnetic scattering," vol. 50, no. 12, pp. 1824–1830.
- [23] R. Adams, "Physical and Analytical Properties of a Stabilized Electric Field Integral Equation," vol. 52, no. 2, pp. 362–372.
- [24] M. Darbas, "Generalized combined field integral equations for the iterative solution of the three-dimensional Maxwell equations," vol. 19, no. 8, pp. 834–839.
- [25] M. B. Stephanson and J.-F. Lee, "Preconditioned Electric Field Integral Equation Using Calderon Identities and Dual Loop/Star Basis Functions," vol. 57, no. 4, pp. 1274–1279.
- [26] Su Yan, Jian-Ming Jin, and Zaiping Nie, "EFIE Analysis of Low-Frequency Problems With Loop-Star Decomposition and Calderon Multiplicative Preconditioner," vol. 58, no. 3, pp. 857–867.
- [27] P. Yla-Oijala, S. P. Kiminki, and S. Jarvenpaa, "Calderon preconditioned surface integral equations for composite objects with junctions," *IEEE Transactions on Antennas and Propagation*, vol. 59, no. 2, pp. 546–554, Feb 2011.
- [28] D. Dobbelaere, D. D. Zutter, J. V. Hese, J. Sercu, T. Boonen, and H. Rogier, "A calderon multiplicative preconditioner for the electromagnetic poincaré–steklov operator of a heterogeneous domain with scattering applications," *Journal of Computational Physics*, vol. 303, pp. 355 – 371, 2015.
- [29] J. Markkanen, "Discrete helmholtz decomposition for electric current volume integral equation formulation," *IEEE Transactions on Antennas and Propagation*, vol. 62, no. 12, pp. 6282–6289, Dec 2014.
- [30] C. L. Epstein and L. Greengard, "Debye sources and the numerical solution of the time harmonic Maxwell equations," vol. 63, no. 4, pp. 413–463.
- [31] W. C. Chew, M. S. Tong, and B. Hu, *Integral Equation Methods for Electromagnetic and Elastic Waves*, vol. 3.
- [32] I. Bogaert, K. Cools, F. P. Andriulli, and H. Bagci, "Low-Frequency Scaling of the Standard and Mixed Magnetic Field and muller Integral Equations," vol. 62, no. 2, pp. 822–831.
- [33] F. Vico, M. Ferrando, L. Greengard, and Z. Gimbutas, "The Decoupled Potential Integral Equation for Time-Harmonic Electromagnetic Scattering," vol. 69, no. 4, pp. 771–812.
- [34] S. Sun, Y. G. Liu, W. C. Chew, and Z. Ma, "Calderon Multiplicative Preconditioned EFIE With Perturbation Method," vol. 61, no. 1, pp. 247–255.
- [35] J. Cheng, R. J. Adams, J. C. Young, and M. A. Khayat, "Augmented EFIE With Normally Constrained Magnetic Field and Static Charge Extraction," vol. 63, no. 11, pp. 4952–4963.
- [36] A. Das and D. Gope, "Modified Separated Potential Integral Equation for Low-Frequency EFIE Conditioning," vol. 64, no. 4, pp. 1394–1403.
- [37] F. P. Andriulli, K. Cools, I. Bogaert, and E. Michielssen, "On a Well-Conditioned Electric Field Integral Operator for Multiply Connected Geometries," vol. 61, no. 4, pp. 2077–2087.
- [38] Y. Beghein, K. Cools, and F. P. Andriulli, "A DC Stable and Large-Time Step Well-Balanced TD-EFIE Based on Quasi-Helmholtz Projectors," vol. 63, no. 7, pp. 3087–3097.
- [39] —, "A DC-Stable, Well-Balanced, Calderon Preconditioned Time Domain Electric Field Integral Equation," vol. 63, no. 12, pp. 5650–5660.
- [40] Y. Beghein, R. Mitharwal, K. Cools, and F. P. Andriulli, "Handling the low-frequency breakdown of the PMCHWT integral equation with the quasi-Helmholtz projectors," in *2015 International Conference on Electromagnetics in Advanced Applications (ICEAA)*, pp. 1534–1537.
- [41] Y. Beghein, K. Cools, and F. P. Andriulli, "A robust and low frequency stable time domain PMCHWT equation," in *2015 International Conference on Electromagnetics in Advanced Applications (ICEAA)*, pp. 954–957.
- [42] W. C. Chew and J. M. Song, "Gedanken Experiments to Understand the Internal Resonance Problems of Electromagnetic Scattering," vol. 27, no. 8, pp. 457–471.
- [43] F. P. Andriulli, I. Bogaert, K. Cools, and E. Michielssen, "A magnetic type integral operator which is stable till extremely low frequencies," in *2014 XXXIth URSI General Assembly and Scientific Symposium (URSI GASS)*, pp. 1–4.
- [44] —, "A well-conditioned combined field integral equation based on quasi-helmholtz projectors," in *2013 International Conference on Electromagnetics in Advanced Applications (ICEAA)*, pp. 644–647.
- [45] A. Buffa and S. Christiansen, "A dual finite element complex on the barycentric refinement," vol. 76, no. 260, pp. 1743–1769.
- [46] K. Cools, F. Andriulli, F. Olyslager, and E. Michielssen, "Nullspaces of MFIE and Calderon Preconditioned EFIE Operators Applied to Toroidal Surfaces," vol. 57, no. 10, pp. 3205–3215.
- [47] D. R. Wilton, "Topological consideration in surface patch and volume cell modeling of electromagnetic scatterers," in *Proc. URSI Int. Symp. Electromagn. Theory*, pp. 65–68.
- [48] A. Napov and Y. Notay, "An Algebraic Multigrid Method with Guaranteed Convergence Rate," vol. 34, no. 2, pp. A1079–A1109.

- [49] K. Cools, F. P. Andriulli, F. Olyslager, and E. Michielssen, "Improving the MFIE's accuracy by using a mixed discretization," in *2009 IEEE Antennas and Propagation Society International Symposium*, pp. 1–4.
- [50] Q. Chen and D. Wilton, "Electromagnetic scattering by three-dimensional arbitrary complex material/conducting bodies," in *Antennas and Propagation Society International Symposium, 1990. AP-S. Merging Technologies for the 90's. Digest.*, pp. 590–593 vol.2.
- [51] I. Bogaert, K. Cools, F. P. Andriulli, and D. De Zutter, "Low frequency scaling of the mixed MFIE for scatterers with a non-simply connected surface," in *Electromagnetics in Advanced Applications (ICEAA), 2011 International Conference On.* IEEE, pp. 951–954.
- [52] I. Bogaert, K. Cools, F. P. Andriulli, J. Peeters, and D. De Zutter, "Low frequency stability of the mixed discretization of the MFIE," in *Antennas and Propagation (EUCAP), Proceedings of the 5th European Conference On.* IEEE, pp. 2463–2465.
- [53] O. Bruno, T. Elling, R. Paffenroth, and C. Turc, "Electromagnetic integral equations requiring small numbers of Krylov-subspace iterations," vol. 228, no. 17, pp. 6169–6183.